WOOD RESEARCH
65 (1): 2020
1-12
doi.org/10.37763/wr.1336-4561/65.1.001012

NOISE REMOVAL IN TREE RADAR B-SCAN IMAGES BASED ON SHEARLET

Jian Wen, Zhaoxi Li, Jiang Xiao
School of Technology, Beijing Forestry University
Beijing, P.R. China

(Received March 2019)

ABSTRACT

There are often many scars and hollows in ancient and famous trees. As a convenient and effective non-destructive testing tool, ground-penetrating (GPR) has a technical advantage in detecting abnormality in trees. But the tree radar images always inherit some extent of noise in them. Thus, denoising is very important to extract useful information from a tree radar image. Shearlet is a directional multi-scale framework, which has been shown effective to identify sparse anisotropic edges even in the presence of a large quantity of noise. This article presents an efficient denoising method based on shearlet applied on the tree radar images. Experimental results on forward modeling and standing trees radar data substantiate that the proposed method has the best denoising performance, especially in preserving the edge information as compared with the other methods which are based on wavelet, curvelet and contourlet.

KEYWORDS: Tree radar image, denoising, the shearlet transform.

INTRODUCTION

The characterization of the structure and the evaluation of the property are essential for managing and protecting ancient and famous trees. In the last decade a considerable amount of non-destructive testing methods has been devoted to the trees. Such as, ultrasonic tomography (Bucur 2005), electrical blocking imaging (Bao and Wang 2013), infrared imaging (Catena 2003), X-ray tomography (Liang et al. 2008) and stress wave (Zhang et al. 2010, Khaled et al. 2012). Even though these methods enable to acquire relatively accurate results, they are expensive, time-consuming and vulnerable to external interference.

Ground-penetrating radar (GPR), as a non-destructive, sufficient detection, simple operation, rapids ampling, high-resolution geophysical tool, has raised a substantial interest in non-destructive testing workers. This tool has been considered reliable for evaluation of geological disaster survey (Tang et al. 2011), concrete bridge decks (Sun et al. 2018), road investigations (Poikajärvi et al. 2012), dielectric structures testing (Ivashov et al. 2018) and

underground structure detection (Lai et al. 2018). Meanwhile, it has been gradually applied to the non destructive testing (NDT) of trees. (Martínez-Sala et al. 2013, Li, W. et al. 2018).

While capturing the tree radar images, noise is automatically introduced. Due to the noise, the interpretability of the tree radar image is been degraded and the extraction of the valuable information is difficult. Thus, the denoising of a tree radar image is one of the most important and basic steps in tree radar image processing.

Large numbers of noise filtering algorithms are present in the literature. Non-liner filters such as median (MED) filters are popular techniques for denoising because of their simplicity and low computational cost. The main shortcoming of MED is that it tends to blur image edges that may be especially significant at higher noise levels. Wavelet have been used in a wide variety of image denoising (Goyal and Tiwari 2013, Ghiyamat et al. 2015).The wavelet shows great effect when dealing with 1-D signal with point singularity features as well as good at dealing isolating discontinuities across horizontal or vertical edges for the 2-D image. However, the isotropic nature of the 2DWT atom renders it inefficient for the description of curvilinear singularities, namely the edge-like details in 2-D image. While for the 2-Dimage, the main characteristics were characterized by the edges.

For 2-D signals there is a large class of representations with a further sensitivity to directional information, useful to deal with the problem of the wavelet transform. Here is worth mentioning curvelet, contourlet and shearlet. Tzanis (2015) used the discrete Curvelet transform to remove noise in the 2-D GPR data to recover features associated with spatial scales and geometry. Terrasse et al. (2015) also used the curvelet for pipe detection. A medical image denoising algorithm using contourlet transform was proposed by Satheesh and Prasad (2011), the results showed that the contourlet transform has higher peak signal-to-noise ratio than the wavelet transform. However, the curvelet and contourlet transform subdivides the image into several layers in the frequency domain, which affects the expression of the sparsity of the image to a certain extent. The shearlet representation has many similarities to the curvelet, but with the additional advantage of a simplified mathematical structure.

The shearlet is a new multiple-scale and multiple-direction geometric analysis technique, which provides optimal approximation properties for images with edges and optimally efficient in representing functions with point wise singularities. This method has been successfully applied in many fields. Gao et al. (2015) proposed a new two-stage method by introducing shearlet transform method to the filtering stage for the removal of impulse noise. Since traditional CT reconstruction algorithms result in instability to noise, and may give inaccurate results for small ROI. Bubba et al. (2017) proposed a non smooth convex optimization model based on shearlet regularization to handle this difficulty. Huang et al. (2018) and Cheng et al. (2018) discussed the infrared and visible image fusion based on non-subsampled shearlet transform (NSST) which is used to deal with the lack of detail in the fusion image because of the artifacts. A cascaded framework that presents a fusion approach for multimodal medical information in non-subsampled shearlet (NSST) domain was proposed by Liu et al. (2017) and Singh et al. (2018). Li, L. et al. (2018) developed a novel microscopy mineral image enhancement approach based on NSST according to the multi-scale and multi-direction analysis characteristics of NSST.

The aim of this paper is to present an algorithm which can remove noise and preserve edge information effectively on the tree radar wave image. The shearlet transform is applied on the denoising of forward modeling radar data and standing trees radar data, and compared with the other three algorithms respectively on wavelet, curvelet, contourlet. Although the shearlet is widely used in image processing, it is of great significance for tree radar wave image processing.

MATERIALS AND METHODS

The continuous shearlet transform

A shearlet frame is an affine-like system of function based on the theory of composite wavelets which is generated by the dilation, shearling and translation of a function $\psi \in L^2(R^2)$. The system is defined in Eq. 1.

$$A_{AS}(\psi) = \left\{\psi_{j,l,k}(x) = |detA|^{\frac{j}{2}}\psi\left(S^l A^j x - k\right): j,l \in Z, k \in Z^2\right\} \quad (1)$$

where: j, l and k are scale, direction, and shift parameters, respectively. A - dilation matrix, controls the scale of the shearlets. The shear matrix S is associated to a directional transformation. The matrix A and S defined respectively by Eq. 2:

$$A = \begin{pmatrix} a & 0 \\ 0 & \sqrt{a} \end{pmatrix}, S = \begin{pmatrix} 1 & s \\ 0 & 1 \end{pmatrix} \quad (2)$$

shearlets provide a decomposition of any $L^2(R^2)$ function into its frequency components according to the tiling of frequency domain by such trapezoids. In order to ensure the effect of decomposition in different directions, the frequency plane is partitioned into four cones C_1-C_4 and a centered rectangle R according to the direction. They are defined as Eqs. 3-7:

$$C_1 = \{(\xi_1, \xi_2) \in R^2: \xi_1 \geq 1, |\xi_2/\xi_1| \leq 1\} \quad (3)$$

$$C_2 = \{(\xi_1, \xi_2) \in R^2: \xi_2 \geq 1, |\xi_1/\xi_2| \leq 1\} \quad (4)$$

$$C_3 = \{(\xi_1, \xi_2) \in R^2: \xi_1 \leq -1, |\xi_2/\xi_1| \leq 1\} \quad (5)$$

$$C_4 = \{(\xi_1, \xi_2) \in R^2: \xi_2 \geq -1, |\xi_1/\xi_2| \leq 1\} \quad (6)$$

$$R = \{(\xi_1, \xi_2) \in R^2; \|(\xi_1, \xi_2)\|_\infty < 1\} \quad (7)$$

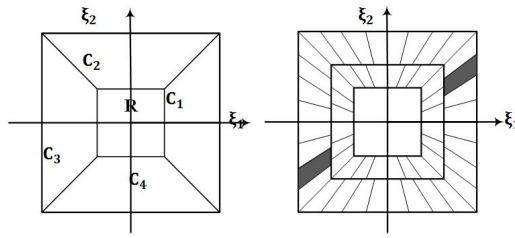

Fig. 1: Shearlet frequency domain subdivision.

As showed in Fig. 1a, the ξ_1,ξ_2 represent the horizontal and vertical coordinates respectively, the low frequency content of a signal is expressed by the rectangle R, C1 and C3 represent the horizontal region and C2 and C4 represent the horizontal vertical region. The gray trapezoid in Fig. 1b represents a pair of shearlet bases in the cones C1 and C3 which were planed.

Since the interest points of an image are associated with high frequencies, the contribution of low-frequency was not considered here.

The shearlet transform SH(f)of a signal $f\in L^2(R^2)$ is defined by Eq. 8.

$$\mathrm{SH}(f)(a,s,t) = \langle f, \psi_{a,s,t}\rangle \tag{8}$$

where: $\langle f, \psi_{a,s,t}\rangle$ is the scalar product in $L^2(R^2)$, which is composed by the scaling fuction $\Phi\in L^2(R^2)$ and the shearing function $\Psi,\Psi \in L^2(R^2)$. Hence, the shearlet transform can also be given by Eqs. 9-11.

$$SH(\varphi,\phi,\bar{\phi}) = \Phi(\varphi)\Psi(\phi)\bar{\Psi}(\bar{\phi}) \tag{9}$$

$$\Phi(\varphi) = \{\varphi_t = \varphi(-t): t \in R^2\} \tag{10}$$

$$\Psi(\phi) = \left\{\phi_{a,s,t} = a^{-\frac{3}{4}}\phi\left(A_a^{-1}S_s^{-1}(-t)\right): a \in (0,1], s \in \left[-\left(1+\sqrt{a}\right), 1+\sqrt{a}\right], t \in R^2\right\} \tag{11}$$

where: a <0being the scale parameter, s ∈ Rbeing the shear parameter, and t ∈ R^2 being the translation parameter. When s<|1|, this produces the cone adapted continuous shearlet transform.

setting:

$$S_{come} = \left\{(a,s,t): a \in (0,1], s \in \left[-\left(1+\sqrt{a}\right), 1+\sqrt{a}\right], t \in R^2\right\} \tag{12}$$

When $\mathrm{SH}_{\varphi,\phi,\bar{\phi}} f: R^2 \times S^2_{come} \to C^3$, we obtain the continuous system in Eqs. 13:

$$\mathrm{SH}_{\varphi,\phi,\bar{\phi}} f\left(t', (a,s,t), (\bar{a},\bar{s},\bar{t})\right) = \left(\langle f, \varphi_{t'}\rangle, \langle f, \phi_{a,s,t}\rangle, \langle f, \phi_{\bar{a},\bar{s},\bar{t}}\rangle\right) \tag{13}$$

The discrete shearlet transform

Digital shearlet systems are defined by sampling continuous shearlet systems on a discrete subset of the space of parameters $R_+ \times R^3$ and by sampling the signal on a grid.

For the horizontal cones C1 and C3, S^D_{come} is discretized as Eqs. 14.

$$S^D_{come} = \left\{\left(2^{-j}, k2^{-j/2}\right), S_{2^{-j/2}k}A_{2^{-j}}M_c m: j \geq 0, k \in \left\{-\left[2^{j/2}\right], \cdots, \left[2^{j/2}\right]\right\}, m \in Z^2\right\} \tag{14}$$

where: c = (c_1, c_2) ∈ $(R^+)^2$ denoted the sampling parameter, M denoted sampling matrix.

For vertical areas, a similar processing method can be used for discretization processing. Hence, the discrete shearlet transform was considered as the following formulations:

$$\mathrm{SH}^D(c;\varphi,\phi,\bar{\phi}) = \Phi(c_1,\varphi)\Psi(c,\phi)\bar{\Psi}(c,\bar{\phi} \tag{15}$$

$$\Phi(c_1,\varphi) = \{\varphi_m = \varphi(-c_1 m): m \in Z^2\} \tag{16}$$

$$\Psi(c,\phi) = \left\{\phi_{j,k,m} = 2^{-3j/4}\phi(S_{-k}A_{2j} - M_c m): j \geq 0, |k| \leq \left[2^{j/2}\right], m \in Z^2\right\} \tag{17}$$

setting:

$$\Lambda_{come} = \left\{(j,k,m): j \geq 0, |k| \leq 2^{j/2}, m \in Z^2\right\} \tag{18}$$

When $\mathrm{SH}^{D}_{\varphi,\phi,\bar{\phi}} f: Z^2 \times \Lambda^2_{come} \to C^3$, we obtain the discrete system in Eqs. 19.

$$\mathrm{SH}^{D}_{\varphi,\phi,\bar{\phi}} f\left(m',(j,k,m),(\bar{j},\bar{k},\bar{m})\right) = (\langle f,\varphi_{m'}\rangle,\langle f,\phi_{j,k,m}\rangle,\langle f,\phi_{\bar{j},\bar{k},\bar{m}}\rangle) \tag{19}$$

where: $f \in L^2(R^2)$.

Denoising with the shearlet transform

In this section, the process of denoising with the shearlet transform was introduced. Given the tree radar images M=G+N, where G represents the GPR signals, N represents noise. The M is transformed into low frequency and high frequency coefficients at each scale using DST. The high frequency coefficients then distribute in different scales and directions.

Since the energy of the tree radar image signal is stronger than the energy of random noise, the shearlet coefficients of the tree radar image signal is bigger than which of noise. Then making the shearlet coefficients which are smaller than the threshold value become zero. In this way, random noise can be removed. Thus, we choose the soft threshold function, which is defined by Eq. 20:

$$T_{soft}(w_{j,k}) = \begin{cases} 0 & |w_{j,k}| < \lambda \\ sgn(w_{j,k}) * (|w_{j,k}| - \lambda) & |w_{j,k}| \geq \lambda \end{cases} \tag{20}$$

where: *sgn* denotes symbolic function, T_{soft} denotes the decomposition coefficient after the soft threshold operation. The threshold values λ is calculated by The Visu Shrink threshold which is defined as Eq. 21:

$$\lambda = \sigma_n \sqrt{2\,ln\,N} \tag{21}$$

where: σ_n is the standard deviation of Gaussian white noise with a mean of zero. N is the length of the signal.

After threshold processing, reconstructing and adding high frequency coefficient at different scales to obtain high frequency coefficients, as below:

$$\widehat{\mathrm{G}} = S^{-1} T_{soft}(w_{j,k}) \tag{22}$$

Finally, combine the decomposed low frequency coefficients with the reconstructed high frequency coefficients; we can obtain an image after noise removal which is given as Eq. 23

$$\widehat{\mathrm{M}} = \widehat{\mathrm{G}} + \mathrm{N} \tag{23}$$

RESULTS AND DISCUSSION

Performance measure

In order to evaluate the efficiency of the shearlet-based denoising method on tree radar image. The performance of the proposed method was extensively compared qualitatively and quantitatively with some existing methods, including wavelet, curvelet and contourlet.

To judge the quantitative performance, three standard measures such as signal-to-noise ratio (SNR), i.e. the ratio of image information and noise contained in the image, the peak signal-to-noise ratio (PSNR) and the edge preservation index (EPI) were used.

These can be considered as indicators of the performance of the filtering method well-denoised by identifying the parameters which results in the highest SNR and PSNR and the value of EPI should be close to 1. The measures are defined in Eqs. 24-27 respectively.

$$\mathrm{SNR} = 20 \times \log_{10}\left\{\sum_{i=1}^{i=N}\sum_{j=1}^{j=M}\frac{rawrata^2(i,j)}{prodata^2(i,j)-rawdata^2(i,j)}\right\}\ (\mathrm{dB}) \tag{24}$$

$$\mathrm{PSNR} = 20 \times \log_{10}\left\{\frac{\max\left(rawdata^2(i,j)\right)}{\sqrt{MSE}}\right\}\ (\mathrm{dB}) \tag{25}$$

$$\mathrm{MSE} = \frac{\sum_{i=1}^{i=N}\sum_{j=1}^{j=M}(prodata^2(i,j)-rawdata^2(i,j))}{M\times N}\ (P^2) \tag{26}$$

$$\mathrm{EPI} = \sum_i \sum_j \frac{|I_{pro}(i,j+1)-I_{pro}(i,j)|}{|I_{raw}(i,i+1)-I_{raw}(i,j)|} \tag{27}$$

where, raw data represents the original image and prodata represents the denoised image. M×N describes the size of GPR data.

Though PSNR can measure the intensity difference between the images, the visual analysis of the image quality is extremely important for subjective evaluation. For quantitative performance measure, these methods were applied on the forward modeling radar data and standing trees radar data. In the experiment, all the methods are implemented in MATLAB2016.

Experiment on forward data

The experiment was performed on the forward data firstly. The tree radar image was simulated by finite-difference tine-domain (FDTD) method, and GprMax software which is an open source software that simulates electromagnetic wave propagation was employed.

The model design of tree trunk B-san image is as follows. The geological background is wood, and the hollow is air. The radius of the tree model is 60 cm. The electrical conductivity of bark is 5 $S{\cdot}m^{-1}$, the electrical conductivity of sapwood is 11 $S{\cdot}m^{-1}$, the electrical conductivity of heartwood is 13 $S{\cdot}m^{-1}$. To better mimic the appearance of the real tree trunk image, there are two defects designed in the tree trunk, one is a scar A on sapwood whose electrical conductivity is 6 $S{\cdot}m^{-1}$, the other one is a hollow B on heartwood whose electrical conductivity is 16 $S{\cdot}m^{-1}$. The tree radar B-scan image model produced by GprMax is showed in Fig. 2. It can be noted that different defects represent different curve characteristics.

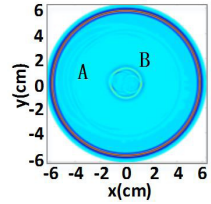

Fig. 2: Forward tree radar B-scan image model.

The forward tree radar B-scan image was noise-free while the image actually acquired was disturbed by various factors and contained noise. The most simplifying assumption while solving image noise problems has been contaminated with Additive White Gaussian Noise. Sothe Additive white Gaussian Noise is taken as the model noise in this work.

The noisy tree radar B-scan image is showed in Fig. 3a. As shown in Fig. 3a, the

characteristics of defect inside the tree trunk was covered by noise, especially the characteristics of scar A which was almost blur.

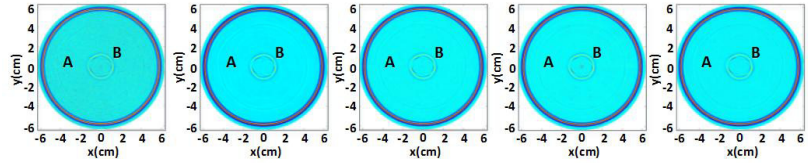

Fig. 3: Denoising results for the forward tree radar B-scan image (a) Noisy image (b) Results using Wavelet (c) Results using Curvelet (d) Results using Contourlet (e) Results using Shearlet.

Fig. 3 shows the comparison with the other three methods; we found that all of the denoising methods can effectively enhance visual quality of the defect characteristics from noise. However, the shearlet-based method significantly reduce the noise with remaining the edge features of defects, compared to the wavelet-based method, whose edge features with more saw tooth sensation. Whereas with the results of curvelet and contourlet, the differences of the visual effects at a glance are little, and our evaluations are sometimes inferior.

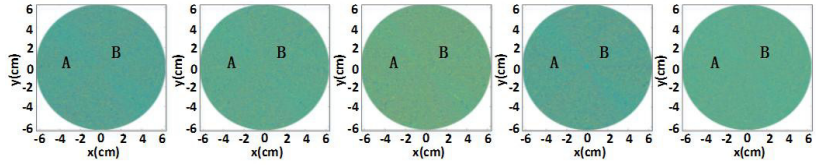

Fig. 4: Difference between noisy image and denoised image (a) Original noise (b) Difference of Wavelet (c) Difference of Curvelet (d) Difference of Contourlet (e) Difference of Shearlet.

The other evaluation value comes from the difference between noisy image and denoised image as shown in Fig. 4. The difference images of shearlet-based method are not over-smoothed unlike the other' difference and have significantly closer similarity to the original noisy image than the other method. Particularly for the curvelet and contourlet-based methods, the difference images are over-smoothed, this indicates that of which the noise removal is not enough. It shows that the shearlet-based denoising performs best ability to reduce noise while preserving the edge features of defects for the noisy tree radar forward image.

The contents of SNR, PSNR and EPI in the forward tree radar data of different denoising methods are listed in Tab. 1. Quantitatively, our proposed method gives highest PSNR and SNR results than those of the other compared methods. Moreover, the EPI of shearlet-based was closest to 1. Thus, it confirms that the proposed method not only has best denoising performance, it also keeps the images more faithful to the noise-free images after denoising.

Tab. 1: The digital results of 4 denoising methods in forward tree radar B-scan image.

Parameter	Wavelet	Curvelet	Contourlet	Shearlet
PSNR	65.1270	67.0891	66.3956	68.4431
SNR	31.2289	36.2057	34.7803	53.6284
EPI	0.0520	0.2601	0.3073	0.3186

Experiment on standing trees radar data

The tree radar used in this paper is the TRU tree radar detection system produced by TreeWin Company of the United States. The tree radar detection system mainly includes two parts: a radar wave medium coupling antenna and a data collector. The medium-coupled antenna internally includes a set of transmit-receive antenna pairs and radar wave generating circuits for transmitting and receiving radar waves. The data collector is used to set the mode of the radar wave detection system. Such as the root detection or trunk detection, this paper mainly uses the TRU detection system to detect the defects inside the trunk. The data collector is also used to set the scan diameter of the probe since selecting the appropriate measurement diameter can make the test results more accurate. The data collector stores the echo signals received in a binary data format in a file with a suffix of *.dzt for subsequent data reading and processing.

Fig. 5 shows hundreds of years old tree at south of Jiehu Bridge in Summer Palace. In this paper, radar wave scanning was performed on the cross sections of the trunks at 0.6 m, 0.9 m, 1.5 m and 1.8 m from the ground. The red vertical line was the starting position of scanning. The perimeters of cross sections were 5.21 m, 4.67 m, 4.91 m, 5.08 m separately. Therefore, the value of the scanning diameter 130 cm was used in this experiment.

Fig. 5: The old willow at south of Jiehu Bridge in Summer Palace.

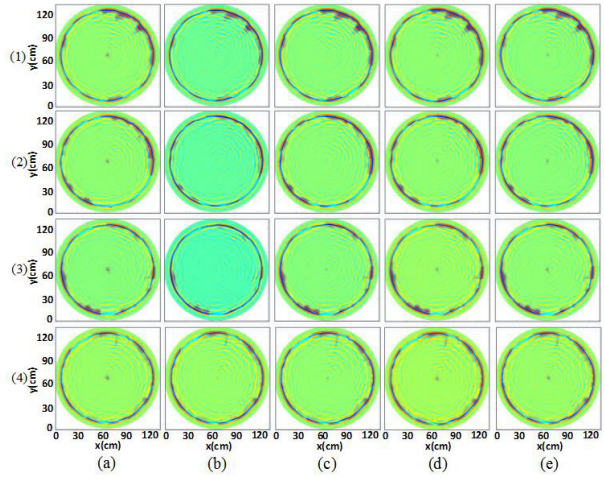

Fig. 6: Denoising results for the standing tree radar B-scan image: (a) Scanning image of 0.6 m, 0.9 m, 1.5 m, 1.8 m (b) Results using Wavelet (c) Results using Curvelet (d) Results using Contourlet (e) Results using Shearlet.

The scanning results of 0.6 m, 0.9 m, 1.5 m and 1.8 m are shown in the first column of Fig. 6 (1)-(4) from top to bottom. It shows that the ancient tree has suffered from a large area of hollows, scars and other defects. Four denoising methods were performed for the tree radar images of four scanning heights respectively, which were showed in Fig. 6b-e. Furthermore, the quantitative performances are listed in Tab. 2.

Tab. 2: The digital results in tree radar images of four cross sectional heights by fourdenoising methods for standing tree.

Height	**0.6m**			**0.9m**			**1.5m**			**1.8m**		
Parameter	PSNR	SNR	EPI	PSNR	SNR	EPI	PSNR	SNR	EPI	PSNR	SNR	EPI
Wavelet	65.037	19.933	0.251	65.024	18.935	0.251	64.928	17.470	0.205	64.928	18.170	0.211
Curvelet	65.908	22.679	0.304	66.271	21.655	0.304	66.748	21.502	0.419	66.854	22.374	0.359
Contourlet	66.297	21.829	0.350	65.978	21.014	0.350	66.086	20.078	0.362	66.037	20.343	0.387
Shearlet	68.717	27.535	0.428	68.697	26.538	0.429	68.742	25.462	0.436	68.716	26.045	0.428

As indicated by the results, the contourlet and shearlet-based methods perform better in denoising. In addition, the shearlet-based method outperforms the other three methods both in noisy removal quality index and edge preservation index. Thus, it confirms the validity of the proposed method in both appearance and numerical evaluation in comparison with the other three methods.

The multi-scale analysis is widely used in image processing by other author, such as in reinforced concrete, underground pipeline, medical image and so on. But the application of multi-scale analysis in standing trees in this article is of great significance. Comparison of four common filtering methods is presented in this article. Through appearance and numerical evaluation, the conclusion is concluded that the shearlet transform is the most suitable noise removal algorithm in non-destructive testing of standing trees.

CONCLUSIONS

In this paper, the shearlet-based denoising method was proposed for the tree radar image. The continuous shearlet transform and a discrete setting were presented, then the denoising with shearlet transform was discussed on image.

Two experiments were performed on noise images, the first one was forward modeling tree radar data affected by the Additive white Gaussian Noise. On one hand the numerical evaluation results achieved by the proposed method surpasses the other three methods by a large margin, on the other hand the edges and details preserved by the proposed method are obviously better than the other methods and most faithful to the noise free image. The second one was tree radar B-scan images acquired by the standing trees where the images included noise effects. The proposed method shows significantly better performance over the other three methods by achieving satisfactory results in both numerical and visual evaluation.

Future areas of further development of our research include the expansion of our method to the denoising of the tree radar images and such work is currently underway.

ACKNOWLEDGEMENT

This research is financially supported by the Supported by Beijing Natural Science Foundation (6202023) and the National Natural Science Foundations of China (Grant No.31600589). The authors have no conflict of interest to declare.

REFERENCES

1. Bao, Z., Wang, H., 2013: Application of electrical resistance testing method in detection of decay in standing trees. College of Engineering and Technology 29 (6): 47-51.
2. Bubba, T.A., Porta, F., Zanghirati, G., Bonettini, S., 2017: A nonsmooth regularization approach based on shearlets for Poisson noise removal in ROI tomography. Applied Mathematics & Computation 318: 131- 152.
3. Bucur, V., 2005: Ultrasonic techniques for nondestructive testing of standing trees. Ultrasonics 43(3): 237-239.
4. Catena, A., 2003: Thermography reveals hidden tree decay. Arboricultural Association Journal 27 (1): 27-42.
5. Cheng, B., Jin, L., Li, G., 2018: Adaptive fusion framework of infrared and visual image using saliency detection and improved dual-channel PCNN in the LNSST domain. Infrared Physics & Technology 92: 30-43.
6. Gao, G., Liu, Y., Labate, D., 2015: A two-stage shearlet-based approach for the removal of random-valued impulse noise in images. Journal of Visual Communication and Image Representation 32: 83-94.
7. Ghiyamat, A., Shafri, H.Z.M., Mahdiraji, G.A., Ashurov, R., Mansour, S., 2015: Airborne hyperspectral discrimination of tree species with different ages using discrete wavelet transform. International Journal of Remote Sensing 36 (1): 318-342.
8. Goyal, P., Tiwari, V.M., 2013: Application of the continuous wavelet transform of gravity and magnetic data to estimate sub-basalt sediment thickness. Geophysical Prospecting 62 (1): 148-157.
9. Huang, Y., Bi, D., Wu, D., 2018: Infrared and visible image fusion based on different constraints in the non-subsampled shearlet transform domain. Sensors 18 (4): 1169.
10. Ivashov, S.I., Bugaev, A.S. , Zhuravlev, A.V. , Razevig, V.V., Chizh, M.A., Ivashov, A.I., 2018: Holographic subsurface radar technique for nondestructive testing of dielectric structures. Technical Physics 63 (2): 260-267.
11. Horáček, P., Tippner, J., Hassan, K.T., 2012: Nondestructive evaluation of static bending properties of scots pine wood using stress wave technique. Wood Research 57(3): 359-366.
12. Poikajärvi, J., Peisa, K., Herronen, T., Aursand, P.O., Maijala, P., Narbro, A., 2012: GPR in road investigations – equipment tests and quality assurance of new asphalt pavement. Nondestructive Testing Communications 27 (3): 293-303.
13. Lai, W., Chang, R.K.W., Sham, J.F.C., 2018: A blind test of nondestructive underground void detection by ground penetrating radar (GPR). Journal of Applied Geophysics 149: 10-17.
14. Liang, S., Wang, X., Cai, Z., Ross, R.J., Bruce, R., Fu, A., 2008: Elastic wave tomography in standing tree decay detection. Research Institute of Wood Industry: 44 (5): 109-114.
15. Li, L., Si, Y., Jia, Z., 2018: Microscopy mineral image enhancement based on improved adaptive threshold in nonsubsampled shearlet transform domain. AIP Advances 8(3): 035002.

16. Li, W., Wen, J., Xiao, Z., Xu, S.X., 2018: Application of ground-penetrating radar for detecting internal anomalies in tree trunks with irregular contours. Sensors 18(2): 649.
17. Liu, X., Mei, W., Du, H., 2017: Structure tensor and nonsubsampled shearlet transform based algorithm for CT and MRI image fusion. Neurocomputing 235: 131-139.
18. Martínez-Sala, R., Rodríguez-Abad, I., Barra, R.D., Capuz-Lladró, R., 2013: Assessment of the dielectric anisotropy in timber using the nondestructive GPR technique. Construction & Building Materials 38: 903-911.
19. Satheesh, S., Prasad, K., 2011: Medical image denoising using adaptive threshold based on contourlet transform. Advanced Computing an International Journal 2 (2): 52-58.
20. Singh, S., Anand, R.S., Gupta, D., 2018: CT and MR image information fusion scheme using a cascaded framework in ripplet and NSST domain. IET Image Processing 12(5): 696-707.
21. Sun, H., Pashoutani, S., Zhu, J., 2018: Nondestructive evaluation of concrete bridge decks with automated acoustic scanning system and ground penetrating radar. Sensors 18(6): 1955.
22. Tang, X., Sun, T., Tang, Z., Zhou, Z., Wei, B., 2011: Geological disaster survey based on curvelet transform with borehole ground penetrating radar in Tonglushan old mine site. Journal of Environmental Sciences 23 (Supplement): S78 - S83.
23. Tzanis, A., 2015: The curvelet transform in the analysis of 2-D GPR data: Signal enhancement and extraction of orientation-and-scale-dependent information. Journal of Applied Geophysics 115: 145-170.
24. Terrasse, G., Nicolas, J.M., Trouve, E., Drouet, E., 2015: Application of the curvelet transform for pipe detection in GPR images, Geoscience and Remote Sensing Symposium. IEEE 2015: 4308- 4311.
25. Zhang, H., Wang, C., Su, J., Robert, J.R, 2010: Investigation of stress wave propagation mechanism in American red pine trees. Journal of Beijing Forestry University 32(2): 145-148.

Jian Wen, Zhaoxi Li, Jiang Xiao*
School of Technology
Beijing Forestry University
Beijing 100083, P.R. China
*Corresponding author: XIAOJIANG56@126.COM